International Journal of Digital Earth

ISSN: 1753-8947 (Print) 1753-8955 (Online) Journal homepage: www.tandfonline.com/journals/tjde20

Comparison of UAV-LiDAR-driven biomass estimation approaches in planted forests with different management

Yuwen Fu, Wang Li, Wensheng Duan, Jie Bai, Li Wang & Zheng Niu

To cite this article: Yuwen Fu, Wang Li, Wensheng Duan, Jie Bai, Li Wang & Zheng Niu (2025) Comparison of UAV-LiDAR-driven biomass estimation approaches in planted forests with different management, International Journal of Digital Earth, 18:2, 2576910, DOI: 10.1080/17538947.2025.2576910

To link to this article: https://doi.org/10.1080/17538947.2025.2576910

Published online: 03 Nov 2025.

INTERNATIONAL JOURNAL OF DIGITAL EARTH
2025, VOL. 18, NO. 02, 2576910
https://doi.org/10.1080/17538947.2025.2576910

RESEARCH ARTICLE

OPEN ACCESS Check for updates

Comparison of UAV-LiDAR-driven biomass estimation approaches in planted forests with different management

Yuwen Fu[a,b], Wang Li[a,b,c], Wensheng Duan[a], Jie Bai[d], Li Wang[a] and Zheng Niu[a,b]

[a]Key Laboratory of Remote Sensing and Digital Earth & International Research Center of Big Data for Sustainable Development Goals (CBAS), Aerospace Information Research Institute, Beijing, People's Republic of China; [b]University of Chinese Academy of Sciences, Beijing, People's Republic of China; [c]Institute for Meteorology and Climate Research (IMK-IFU), Karlsruhe Institute of Technology, Garmisch-Partenkirchen, Germany; [d]School of Resources and Environment, University of Electronic Science and Technology of China, Chengdu, People's Republic of China

ABSTRACT

Planted forests play a crucial role in forest restoration and carbon sequestration. However, different management practices in planted forests can alter forest structure and composition, potentially affecting UAV-LiDAR-based biomass estimation. This study evaluated tree-centric, object-based, and area-based approaches in both managed planted forests (MPF) and unmanaged planted forests (UPF). Furthermore, an object biomass index (OBI) was developed for the object-based approach to better capture the structural complexity of forest objects. We then compared the selected metrics and estimation accuracy of the three approaches across forests with different management types. The results showed that in MPF, metrics characterizing canopy height and horizontal structure were more important. Whereas in the UPF, metrics capturing fine-scale structural details contributed to a more accurate biomass estimation. Across all approaches, higher performance was observed in MPF subjected to intensive management. Among the three approaches, the proposed object-based approach proved to be the most robust, demonstrating its potential to mitigate the effects of individual tree segmentation errors. This study underscores the impact of forest management on UAV-LiDAR-driven biomass estimation approaches in planted forests, and emphasizes the importance of accounting for management regimes when estimating forest biomass at larger scales.

ARTICLE HISTORY
Received 11 February 2025
Accepted 13 October 2025

KEYWORDS
Forest management; planted forests; LIDAR-driven biomass estimation approaches; UAV-LiDAR

1. Introduction

Planted forests, defined as forest ecosystems established by artificial tree planting or seeding, are crucial for providing income and goods, restoring ecosystem services, and mitigating climate change (Food and Agriculture Organization 2020; Abbasi et al. 2023). Forest management strategies influence the structure, composition, function, and biomass accumulation rates of planted forests (Erb et al. 2018; Li et al. 2024). Monoculture plantations, characterized by intensive management, consist of a single tree species and exhibit a simplified structure (Scheeres et al. 2023). Although monoculture plantations have been promoted for the restoration of forested areas worldwide, they exhibit low biodiversity and limited productivity (Zhang et al. 2021). With the shift in restoration policies for planted forests from area expansion to stand productivity and quality enhancement, multipurpose management and biodiversity-rich mixed forests have gained more attention (Liu, Wu, and Wang 2014). Compared with traditional management-intensive monoculture plantations, planted forests with little management allow natural regeneration of other tree species into the canopy or shrub layers (Scheeres et al. 2023). Multispecies plantations tend to have taller, thicker trees and achieve higher biomass accumulation than monocultures because of the complementarity among species (Feng et al. 2022; Hulvey et al. 2013). Monitoring forest structure and biomass in planted forests with different management types is crucial for evaluating the

CONTACT Wang Li liwang@aircas.ac.cn Key Laboratory of Remote Sensing and Digital Earth & International Research Center of Big Data for Sustainable Development Goals (CBAS), Aerospace Information Research Institute, Beijing 100101, People's Republic of China

effects of forest management and for maximizing the benefits of plantations for restoration and conservation, with environmental significance for carbon sequestration and biodiversity conservation, as well as economic relevance for sustainable forest management and carbon trading (Li et al. 2023; Yu et al. 2024).

Traditional field methods for forest biomass estimation are mainly based on tree metrics (e.g. species, diameter at breast height (DBH), and tree height) measured in situ and allometric scaling models (ASM) calibrated on destructively harvested individuals (Chave et al. 2005; Jucker et al. 2017). Although field-based approaches have been widely used to estimate forest biomass, they are costly, labor-intensive, and largely constrained by spatial extent (Coops et al. 2021; Liang et al. 2022). Airborne laser scanning (ALS) has been widely used in forest inventories to provide forest structural information at a landscape scale (Bai et al. 2024; Campbell et al. 2023; Li et al. 2020). However, in most surveys, the point densities of ALS datasets are lower than 20 pulses m^{-2}, which makes it difficult to detect fine-scale structural information, such as tree-level attributes in complex forest conditions (Pearse et al. 2019; Qi et al. 2022). Compared with ALS, unmanned aerial vehicle-based laser scanning (ULS) can acquire more detailed point clouds ranging between 60 and 1500 points m^{-2} (Vandendaele et al. 2021). These high sampling densities enable more precise detection of tree structural attributes at a finer scale and further improve the biomass estimation accuracy (Li et al. 2016; Liang et al. 2019; Pearse et al. 2019).

LiDAR-driven biomass estimation approaches can be classified into two main categories: area-based and tree-centric approaches. Area-based approaches link plot-scale biomass to forest structure metrics derived from point clouds using statistical models (Coomes et al. 2017; Latifi et al. 2015). Tree-centric approaches rely on individual tree segmentation to extract tree-level metrics, from which biomass can be estimated using ASM or statistical models (Brede et al. 2022; Campbell et al. 2023; Wang et al. 2021). Compared with area-based approaches, tree-centric methods are conceptually closer to field-based inventory techniques and can provide more detailed structural and demographic information. Nevertheless, their accuracy is strongly influenced by individual tree segmentation errors, particularly the under-segmentation of multiple trees within dense clusters, which remains a key source of uncertainty (Coomes et al. 2017). Different management types in planted forests lead to varying forest structures and compositions, which may affect the performance of the LiDAR-driven biomass estimation approaches mentioned above. For example, the frequency of thinning affects stem density in forest stands. Monoculture plantations, characterized by intensive active managementsuch as the removal of understory vegetation and short rotation timber, have a simpler structure and composition compared to planted forests managed with close-to-nature principles (Scheeres et al. 2023). Thus, the performance of LiDAR-driven biomass estimation methods is likely to vary across forests with different management types. On the one hand, variations in forest structure resulting from different forest management practices can affect the accuracy of individual tree segmentation. Individual tree segmentation algorithms are subject to great errors when applied to forests with complex structures (Vega et al. 2014). These errors propagate to tree-level metrics, introducing additional uncertainties in biomass modelling. Moreover, when tree-level biomass is aggregated to the plot scale, both under-segmented and over-segmented trees are incorporated in to the estimation, leading to biases in plot-level biomass assessments (Campbell et al. 2023; Coomes et al. 2017). On the other hand, forest management can alter not only the interrelationships among structural attributes but also the associations between structural attributes and biomass. Consequently, the selection of metrics and the generalization of models in both tree- and plot-level biomass modelling can be affected (Knapp et al. 2020). However, it remains unclear how tree- and plot-level biomass estimation approaches differ across forests under varying human management, which brings great uncertainty in the assessment of forest sustainable development and restoration.

In LiDAR-driven biomass estimation approaches, uncertainties arising from individual tree segmentation errors can be mitigated through the object-based approach, which regards under-segmented multi-trees within a clump as a single entity. However, previous object-based studies primarily focused on basic metrics such as height, perimeter, and projected area (Jeronimo et al. 2018; Krofcheck et al. 2016). Few studies have explored new metrics suitable for objects with more complex structures. Therefore, it is necessary to further investigate object-based approaches for biomass estimation.

This study aimed to examine the impact of human management on UAV-LiDAR-derived biomass estimations in planted forests. Specifically, we focused on: (1) investigating how forest structural attributes vary across different biomass estimation approaches and between forests with different management types.

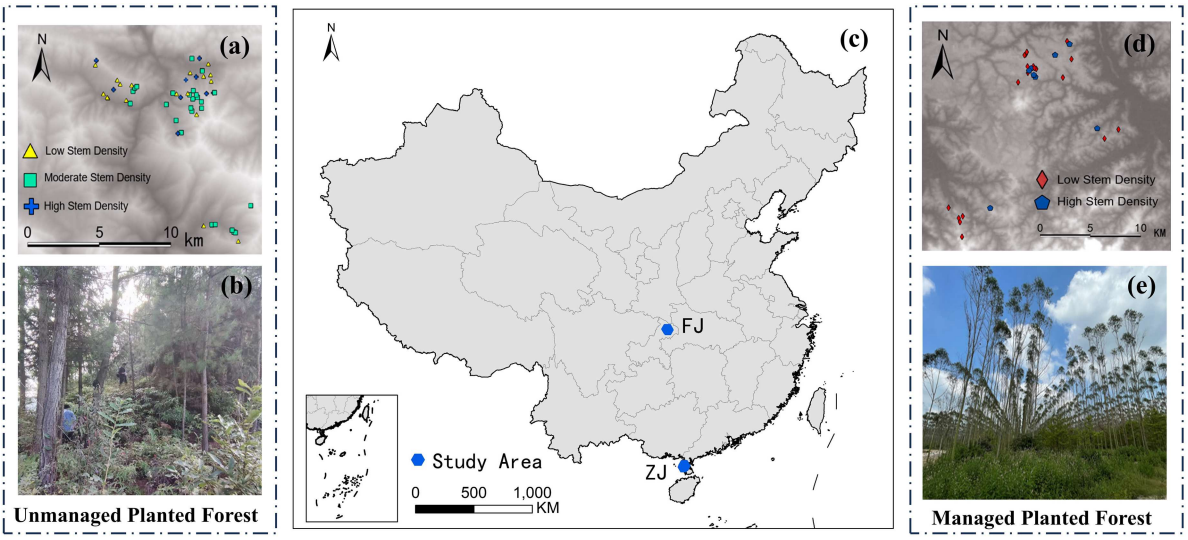

Figure 1. Two types of planted forest with different human management in this study. (a) Presents the distribution of sample plots for the unmanaged planted forest. (b) Is a photo of a planted forest with little management, which has complex structure and composition. (c) is the distribution of study areas in China. (d) Presents the distribution of sample plots for the managed planted forest. (e) Is a photo of a monoculture plantation with intensive management, characterized by a simple vertical structure.

(2) Comparing and assessing the accuracy of biomass estimation in forests with completely different management types using tree-centric, object-based, and area-based approaches, and (3) testing the effectiveness of the object-based approach for biomass estimation to circumvent the impact of individual tree segmentation errors.

2. Materials

2.1. Study sites and sample plots

This study included two types of planted forests under significantly different management. One is a biodiversity-rich mixed forest afforested by aerial sowing that lacks major forest management interventions, referred to as the unmanaged planted forest (UPF) in this study. The other is afforested by planting and is a monoculture plantation with intensive management, referred to as the managed planted forest (MPF). The UPF is located in a forested area of Fengjie, Chongqing, China (31.249° *N*, 109.142° E), where close-to-nature management has led to a structurally complex and mixed-species forest dominated by Masson pine (*Pinus massoniana*), Chinese fir (*Cunninghamia lanceolata*), Cypress (*Cupressus funebris*), and naturally regenerated oak species (Figure 1b). The MPF is located in Zhanjiang, Guangdong, China (20.868° *N*, 109.883° E) and is dominated by eucalyptus trees, one of the fastest-growing and most intensively managed plantation species in China. Active management has resulted in a simplified forest structure with uniform spacing and a homogeneous canopy (Figure 1e). While the two sites differ in climatic conditions, which may influence tree growth rates and biomass accumulation, the observed structural differences are more strongly attributable to contrasting management types than to climate.

According to forest site conditions, such as soil type, slope, and elevation, a stratified sampling was designed at the two study sites. A total of 83 20 m × 20 m sample plots were established in September and October 2023, including 57 plots in the UPF and 26 plots in the MPF. We adopted a minimum DBH threshold of 3 cm to avoid underestimating biomass from abundant small-diameter trees in our study area. The geographic coordinates of individual trees with a DBH ≥ 3 cm were measured using a real-time kinetic (RTK) global navigation satellite system (GNSS). The DBH, height (H), and species of each tree were also recorded. For the dominant trees in the UPF, biomass was calculated using the local species-specific ASM based on DBH and H (Equation 1). For other broadleaf trees, biomass was estimated using a general

equation (Equation 2). For eucalyptus trees in the MPF, biomass was also estimated using the general equation (Equation 2).

$$M = a_{above} \times DBH^{b_{above}} \times H^{c_{above}} + a_{below} \times DBH^{b_{below}} \times H^{c_{below}} \quad (1)$$

$$M = a_{total} \times DBH^{b_{total}} \times H^{c_{total}} \quad (2)$$

where M (kg) represents the biomass of an individual tree, DBH (cm) represents the tree stem diameter, and H (m) is tree height. a_{above}, b_{above}, and c_{above} are local species-specific coefficients for above ground biomass estimation. a_{below}, b_{below}, and c_{below} are local species-specific coefficients for below ground biomass estimation. a_{total}, b_{total}, and c_{total} are the general species-specific coefficients for total biomass estimation. The values of these coefficients are provided in the methodology for the afforestation of carbon sinks of the Greenhouse Gas Certified Emission Reduction Project in China.

The plot-level biomass was calculated by summing the biomass of all trees within each plot. Eight plots were excluded due to limited LiDAR coverage and low point-cloud density. A total of 75 plots (52 plots in the UPF and 23 plots in the MPF) were used for modeling and analysis.

2.2 UAV-LiDAR data

UAV-LiDAR data for the UPF and MPF were acquired in September and October 2023, respectively, using a RIEGL VUX-1LR22 and a mini VUX-1 UAV LiDAR scanner. To reduce the impact of point density on biomass estimation, a resampling strategy was applied to plots with extremely high point densities. The average point density was approximately 200 pts/m^2 in the UPF and 160 pts/m^2 in the MPF. The point clouds were then clipped to the boundaries of sample plots. Noise points were removed using a Statistical Outlier Removal (SOR) algorithm. Cloth Simulation Filtering (CSF) was applied to classify the point clouds into non-ground and ground points (Zhang et al. 2016). Based on digital terrain models (DTMs) with a 0.4-m resolution generated from ground points, we obtained normalized point clouds. These preprocessing procedures were implemented using the CloudCompare software.

3. Methods

In this study, tree-centric, object-based, and area-based approaches were applied in both the UPF and MPF (Figure 2). We compared the performance of these models in estimating biomass at the individual tree/object level as well as at the plot level.

3.1 Tree/object segmentation and matching

We applied different algorithms to the two sites according to their terrain characteristics. In the mountainous UPF, the PTrees algorithm was employed to avoid distortion of point clouds caused by normalization (Vega et al. 2014). By directly processing raw point clouds, PTrees preserved crown geometry and was specifically designed for complex topography. It comprises three main steps: (1) multi-scale segmentation, (2) dynamic apex selection, and (3) final segmentation, with results depending on point kernels of varying sizes. This design makes PTrees more effective in delineating tree crowns under canopy overlap and rugged terrain. In contrast, for the relatively flat MPF, we used the Dalponte (2016) algorithm, which first detects treetops using a local maximum (LM) filter in the canopy height model (CHM) and then applies seeded region-growing with thresholds (TH_CR and TH_SEED) to delineate crown boundaries (Dalponte and Coomes 2016). The window size of the LM filter controls the number of detected trees, making the algorithm more suitable for simpler canopy structures. These site-specific choices ensured the most reliable tree delineation for subsequent tree-level biomass modelling. The object represents clusters of trees, indicating that the segmentation results do not correspond to a single tree (Figure 3). Therefore, compared with tree segmentation, larger parameter values were applied in object segmentation to capture objects containing multiple trees. The PTrees and Dalponte (2016) algorithms were implemented using the lidR plugins and the lidR package (Roussel et al. 2020).

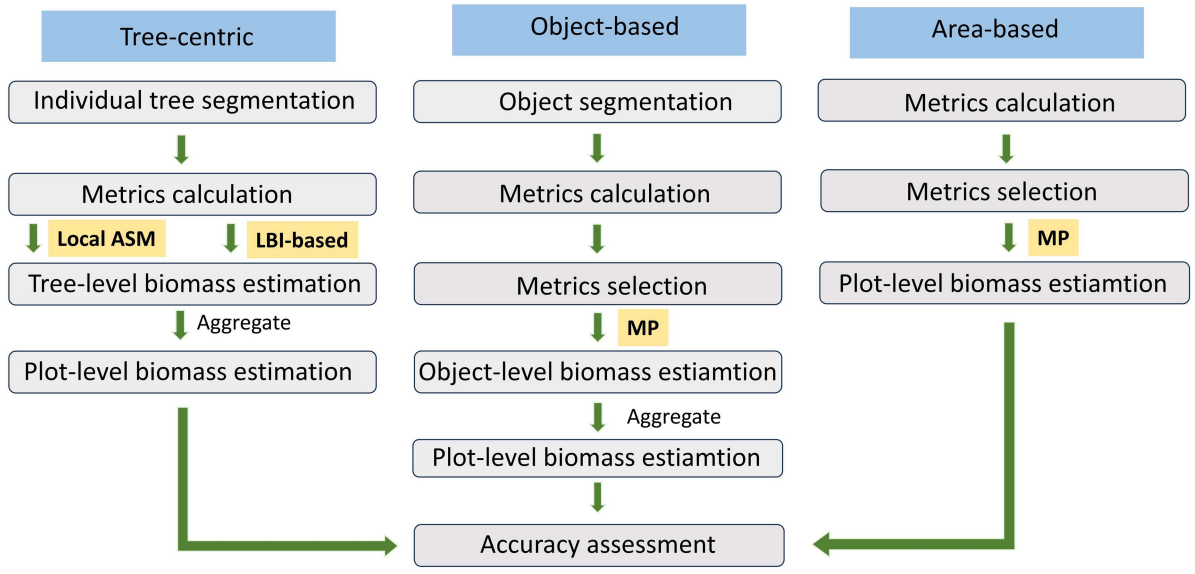

Figure 2. The overall workflow of tree-centric, object-based, and area-based approaches.

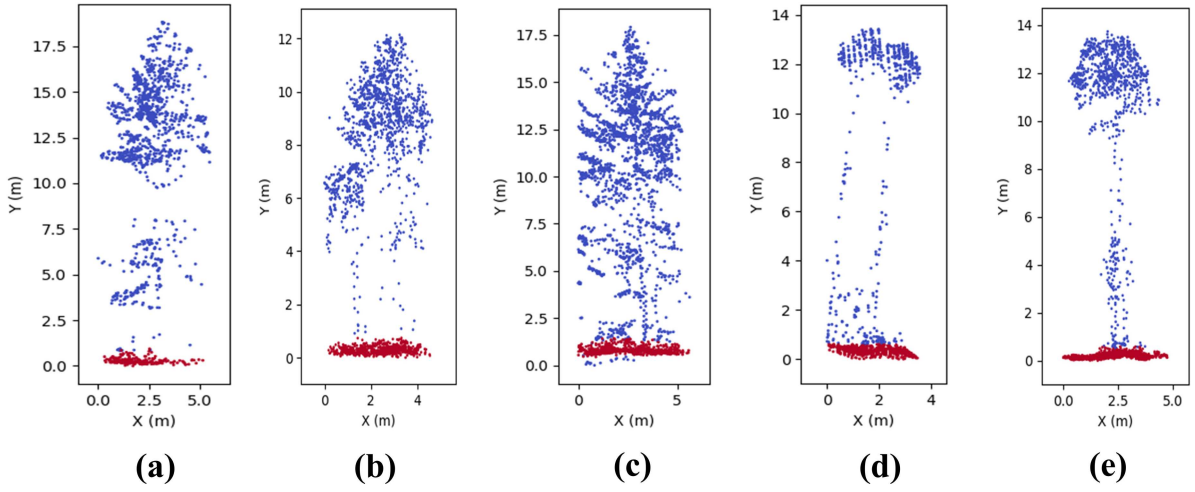

Figure 3. Objects with multiple trees resulting from under-segmentation. (a) and (b) are overlapping tree crowns within a clump; (c), (d) and (e) are multi-story trees.

Field-measured biomass is important for the calibration and validation of tree-centric and object-based models; therefore, we needed to match LiDAR-derived trees or objects to field-measured reference trees. For segmented trees, the matching process was conducted following the method proposed by Eysn et al. (2015). As this approach did not quantify the level of agreement, some deviations remained between the field-measured trees and the segmented trees. To reduce uncertainty, we selected 116 trees in the UPF and 97 trees in the MPF with relatively clear crown morphology from the matched pairs for subsequent analyses. For objects, defined as crown units representing single trees or clusters of trees, traditional automatic matching methods were unsuitable due to the structural complexity of overlapping crowns and variable crown boundaries. We therefore manually matched 219 objects in the UPF and 81 in the MPF to field-measured trees, using spatial location, crown shape, tree height, and overlap with field-mapped positions as matching criteria. These manually matched trees or objects were a reliable reference dataset to establish the tree-level or object-level allometric models, which ensured that subsequent biomass estimates were based on robust structural information. Similar approaches, where manually delineated trees were used to calibrate tree-level biomass models, have also been adopted in previous studies (Coomes et al. 2017).

Table 1. Description of LiDAR-derived metrics for tree-centric, object-based and area-based approaches.

Approach	Metrics type	Metrics name	Description
Tree-centric	Other	H	Tree height
		CD	Crown diameter
		LBI	LiDAR biomass index
Object-based	Other	OBI	Object biomass index
		CE	Canopy entropy
Object-based and Area-based	CHM-based	μ_{CHM}	Average of CHM
		σ_{CHM}	Standard deviation of CHM
		GF	Fraction of CHM cells below 3m
		GC	L-coefficient of variation of heights
	Point-based	$Density_i$	Proportion of points above i height (i = 3,6,9,12,15,18m) to total points
		FHD	Foliage height diversity
		LAI	Leaf area index
	Voxel-based	μ_{HPi}	Average of height at i percentile of a grid (i = 5,10,25,50,75,90)
		σ_{HPi}	Std of height at i percentile of a grid (i = 5,10,25,50,75,90)
		$\mu\mu_{Ht}$	Mean of the mean height of returns within a voxel
		$\eta\mu_{Ht}$	Median of the mean height of returns within a voxel

3.2. Metrics calculation

3.2.1. Tree-centric approach

A range of metrics were derived from individual trees, objects, and plot-level point clouds for biomass estimation (Table 1). Tree height (H), crown diameter (CD), and LiDAR biomass index (LBI) were used in the tree-based approach. Specifically, CD was calculated based on the UAV-LiDAR-derived crown area ($CD = 2 \times \sqrt{CA/\pi}$). LBI is a metric for individual tree biomass estimation developed by Wang et al. (2021) based on TLS data. Du et al. (2023) adapted the TLS-based LBI for ALS data:

$$LBI = \lim_{\Delta H \to 0} \sum_{H=H_B}^{H_T} A(H) \times \Delta H \times H \tag{3}$$

Where H_B is the bottom of the crown, H_T is the tree height, and $A(H)$ is the crown area at a height H.

We set H_B to 1m to avoid interference from shrubs and other low vegetation while ensuring that all tree crowns are captured. The ΔH was 0.5 m, and $A(H)$ was calculated using the Delaunay triangulation method, which were consistent with Du et al (2023).

3.2.2. Object-based approach

Considering the structural complexity and heterogeneous composition of objects, we developed an object biomass index (OBI) for extracting crown structure information from objects containing multiple crowns. The OBI was calculated as the following simplified equation:

$$OBI = \sum_{h} W(h) \times A(h) \times \Delta h \times h \tag{4}$$

where h represents the height, $W(h)$ is the weight at height layer h, $A(h)$ is related to area of the crown at height layer h, and Δh is the thickness of the horizontal slices.

First, we used the robust kernel density estimation (KDE) method to derive the probability density curves of the vertical point distribution and divided the point clouds into slices with a specific height interval of 1m (Figure 4b). The integral over each interval was then computed, and a square root transformation was applied to constrain the weight to a reasonable order of magnitude. Then, for each slice, the point clouds were projected onto the XY-plane and rasterized to 0.1-m grid cells. The probability density $p(x, y)$ also was calculated using KDE. Pixels with a higher number of points exhibited greater values, and the brighter areas corresponded to crown contours composed of point clouds (Figure 4c). A threshold was applied to filter out darker pixels with lower values, and the sum of the brighter pixel was used to estimate the crown area within each slice. Tree crown overlap, however, can lead to under-estimation of object area. To address this, each pixel was weighted based on the number of points in the slice and its probability density $p(x, y)$ at that location, so that pixels in overlapping regions, which

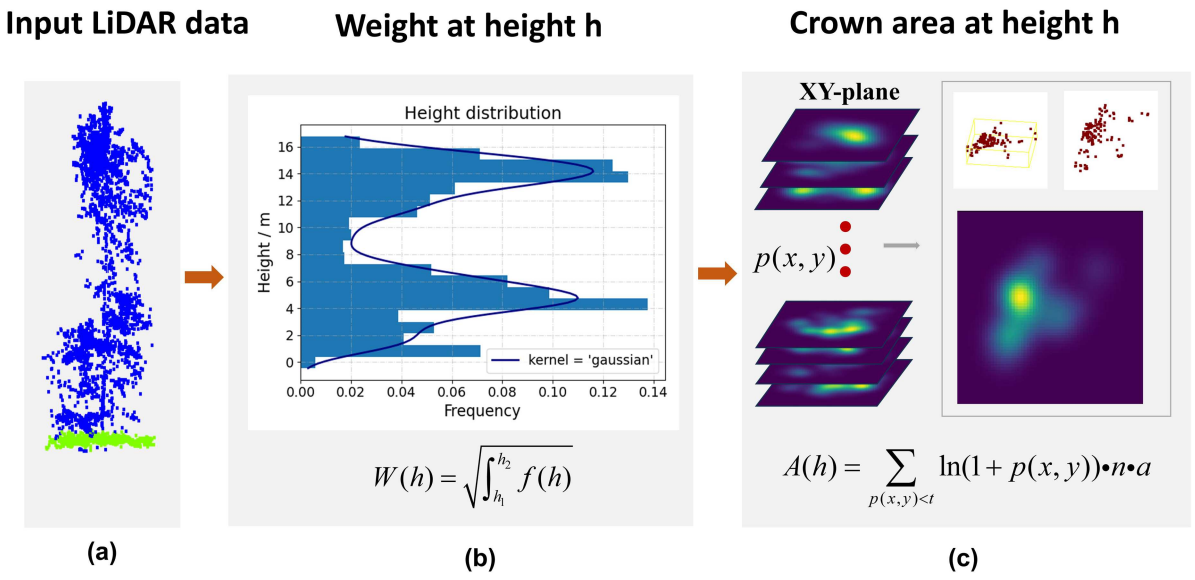

Figure 4. The illustration of OBI. The calculation of OBI has two main parts: the weight and the crown area at height h.

contain more points, contributed proportionally more to the estimated crown area. In summary, $A(h)$ was calculated using the following equation.

$$A(h) = \sum_{p(x,y)<t} \ln(1 + p(x, y)) \times n \times a(x, y) \tag{5}$$

Where $p(x, y)$ denotes the probability density of the pixel at the location (x, y), n is the number of points in the height layer, and a is the pixel area. The parameter t represents the threshold.

In addition, we introduced canopy entropy CE, CE_XY, CE_XZ, and CE_YZ proposed by Liu et al. (2022). These indices can capture variations in forest canopy structural complexity arising from differences in tree density and the number of vertical canopy layers. We also extracted the CHM-based, point-based, and voxel-based metrics (Section 3.2.3).

3.2.3. Area-based approach

For each plot, a suite of LiDAR-derived metrics were calculated, including CHM-based, point-based, and voxel-based metrics (Blackburn, Buscaglia, and Sánchez Meador 2021; Pearse et al. 2019; Scheeres et al. 2023; Whelan et al. 2023).

The CHMs were generated from normalized point clouds at a grid resolution of 0.4 m, and the corresponding metrics were derived from these CHMs Point-based metrics were directly extracted from the normalized point clouds, and included the proportion of point clouds above specified height i relative to the total number of points (i = 3, 6, 9, 12, 15, 18 m), foliage height diversity (FHD), and leaf area index (LAD). Voxel-based metrics, derived from dividing the point cloud space into a 3D grid of smaller volumes, capture both horizontal and vertical variabilities, thereby better characterizing forest structural heterogeneity and supporting the development of a general biomass estimation model (Whelan et al. 2023).

3.3. Metrics selection and biomass modelling

3.3.1. Tree-centric approach

In this study, two individual tree biomass modelling strategies were adopted: a local ASM and an LBI-based model.

A power-law function based on tree height and crown diameter was selected as a local ASM (Jucker et al. 2017). The ASM was fit based on the data from 2,395 trees which demonstrated that the function

Table 2. Biomass model of tree-centric, object-based and area-based approach.

Approach	Model		Calibration dataset
Tree-centric	Local ASM	$\ln(Biomass) = \alpha + \beta \ln(H \times CD)$	116 trees (UPF) 97 trees (MPF)
	LBI-based	$Biomass = k \times H_T^{\beta} \times LBI^{\frac{2\beta}{\alpha}}$	
Object-based	MP	$\ln Biomss = \alpha_0 + \alpha_1 \ln P_1 + \alpha_2 \ln P_2 + \ldots \alpha_n \ln P_n$	219 objects (UPF) 81 objects (MPF)
Area-based	MP	$\ln Biomss = \alpha_0 + \alpha_1 \ln P_1 + \alpha_2 \ln P_2 + \ldots \alpha_n \ln P_n$	52 plots (UPF) 23 plots (MPF)

delivered unbiased estimations. Therefore, we used this function in our study. The local ASM was expressed as follows:

$$\ln(Biomass) = \alpha + \beta \ln(H \times CD) \tag{6}$$

Biomass refers to the individual tree biomass based on field-measured data. H and CD represent tree height and crown diameter, respectively. They were calculated from the individual tree point clouds (Section 3.2.1). α and β are the model coefficients. The model was calibrated using the matched field-measured tree biomass and UAV-LiDAR-derived metrics. Using the calibrated local ASM, the biomass of all segmented trees was estimated. Plot-level biomass was then obtained by summing the biomass of all segmented trees within each plot.

The LBI-based model was expressed as the following model:

$$Biomass = k \times H_T^{\beta} \times LBI^{\frac{2\beta}{\alpha}} \tag{7}$$

Biomass is the individual tree biomass based on field-measured data. H and LBI are tree height and LiDAR biomass index, respectively (Section 3.2.1). k, α, and β are the model coefficients (Du et al. 2023). The model was calibrated using the matched tree dataset (Table 2), and biomass was estimated at both the individual and plot levels.

3.3.2. Object-based approach

We used the multiplicative power (MP) model to predict object biomass. This model has been widely used to predict forest attributes (Næsset and Bjerknes 2001; Whelan et al. 2023).

$$\ln Biomss = \alpha_0 + \alpha_1 \ln P_1 + \alpha_2 \ln P_2 + \ldots \alpha_n \ln P_n \tag{8}$$

Where P_i is the metric derived from the object point clouds (Section 3.2.2), and α_i is the coefficient for P_i. To prevent model overfitting and reduce collinearity, we first calculated the Pearson correlation coefficients between LiDAR metrics (Shi et al. 2018). For metric pairs with $|r| > 0.8$, we removed the metric with lower permutation importance. To further optimize the model performance, we fitted models with all combinations of the remaining metrics and selected the optimal model based on Akaike Information Criterion (AIC) minimization (H. Akaike 1974). Object-level biomass was then estimated using the optimal model, and biomass of objects within the same plot were aggregated to obtain plot-level estimates.

3.3.3. Area-based approach

Similar to the object-based approach, the area-based approach used the multiplicative power (MP) model. The model was calibrated using metrics derived from plot-level point clouds (Section 3.2.3) and the field-measured plot-level biomass.

$$\ln Biomss = \alpha_0 + \alpha_1 \ln P_1 + \alpha_2 \ln P_2 + \ldots \alpha_n \ln P_n \tag{9}$$

Where P_i is the UAV-LiDAR metric and α_i is the coefficient for P_i. Feature selection was performed in the same manner as in the object-based method.

3.3.4. Accuracy assessment

We adopted leave-one-out cross-validation (LOOCV) to assess the performance of the object-, plot-, and tree-centric models. In LOOCV, the model is trained using all but one sample and validated on the remaining sample (Brovelli et al. 2008). This process is repeated until each sample has been used for model validation. In total, 14 modeling results were trained and evaluated in our study: object-based models for object- and plot-level biomass estimation, area-based models for plot-level biomass estimation, and tree-centric models using two methods for individual- and plot-level biomass estimation in both the UPF and MPF. To ensure model generalization, for plot-level biomass estimation derived from object-based and tree-centric approaches, objects or individual trees within the validation sample plot were excluded from the training dataset.

The performance of these models was evaluated using three indicators: coefficient of determination (R^2), root mean square error (RMSE), and relative root mean square error (rRMSE).

$$R^2 = 1 - \frac{\sum_{i=1}^{n}(y_i - \hat{y}_i)^2}{\sum_{i=1}^{n}(y_i - \bar{y})^2} \tag{10}$$

$$RMSE = \sqrt{\frac{\sum_{i=1}^{n}(y_i - \hat{y}_i)^2}{n}} \tag{11}$$

$$rRMSE = \frac{RMSE}{\bar{y}} \tag{12}$$

where y_i and $\hat{y}_i$ are the reference and predicted biomass of the i^{th} sample, respectively, and $\bar{y}$ is the mean biomass of all samples. For the tree- and object-level biomass validation, the reference biomass corresponded to the field-measured values of the matched tree and object datasets (Section 3.1). For the plot-level biomass validation, the reference biomass was taken from the corresponding field measurements (Section 2.1).

4. Results

4.1. Metrics selection with object-based and area-based approach

The final selected metrics and their permutation importance varied across modelling approaches and forest management types (Figure 5). For the object-based model in the MPF, the metrics retained in the optimal model after feature selection were $Density_{15}$, OBI, $Density_{12}$, CE_XY, and $\mu_{CHM.}$ In the UPF, four metrics were retained in the optimal object-based model: OBI, CE_XY, μ_{HP75} and μ_{HP10}. For the area-based model in the MPF, the optimal model retained the CHM-related metric σ_{CHM}, GF, and μ_{HP10}. In the UPF, the optimal model retained μ_{HP75}, σ_{HP75} and LAI.

4.2. Tree/object-level biomass estimation

Overall, the accuracy of all approaches was higher in the MPF, which can be attributed to the relatively simpler structure and composition of the MPF. Among the three approaches, the LBI-based approach performed best in the MPF with R^2 of 0.92 and rRMSE of 19.76%, followed by the object-based approach and the local ASM approach, which achieved R^2 of 0.79 and 0.55, respectively (Figure 6a). As forest structure and composition became more complex in the UPF, the advantages of the object-based approach emerged. In the UPF, the object-based approach outperformed the other two tree-centric models, with an R^2 of 0.76 (Figure 6b).

4.3. Plot-level biomass estimation

In the MPF, the area-based approach achieved the highest accuracy, with an R^2 of 0.90 and an rRMSE of 17.45%. The R^2 values of the object-based, local ASM-, and LBI-based approaches were 0.87, 0.56, and

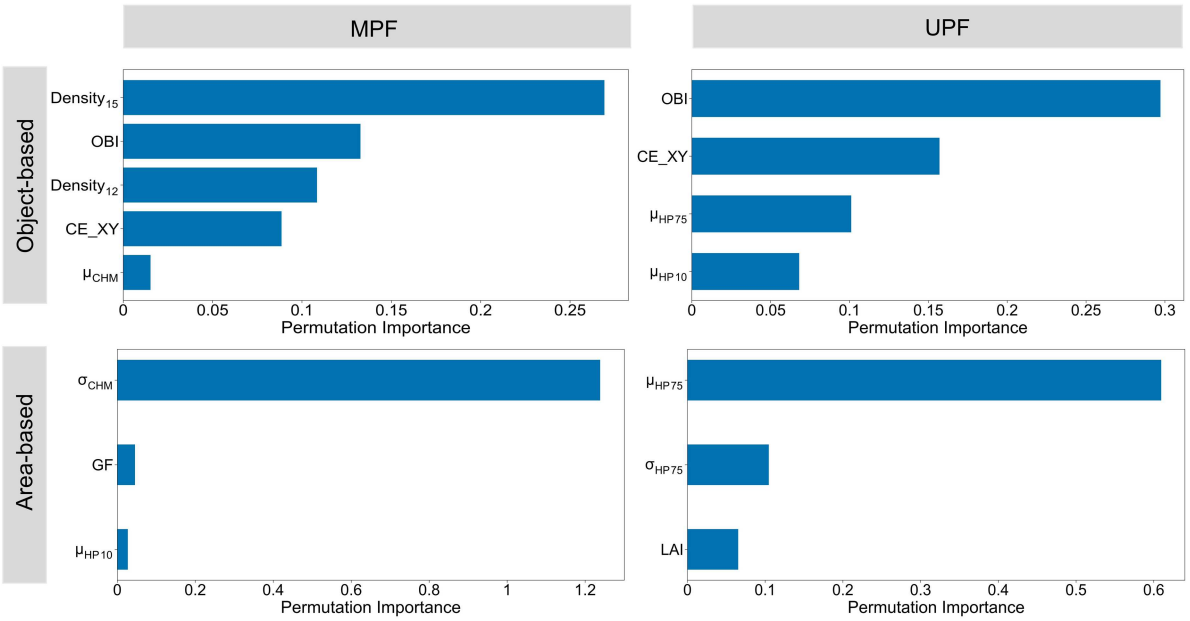

Figure 5. Permutation importance for metrics of the object-based and area-based MP models in the UPF and MPF.

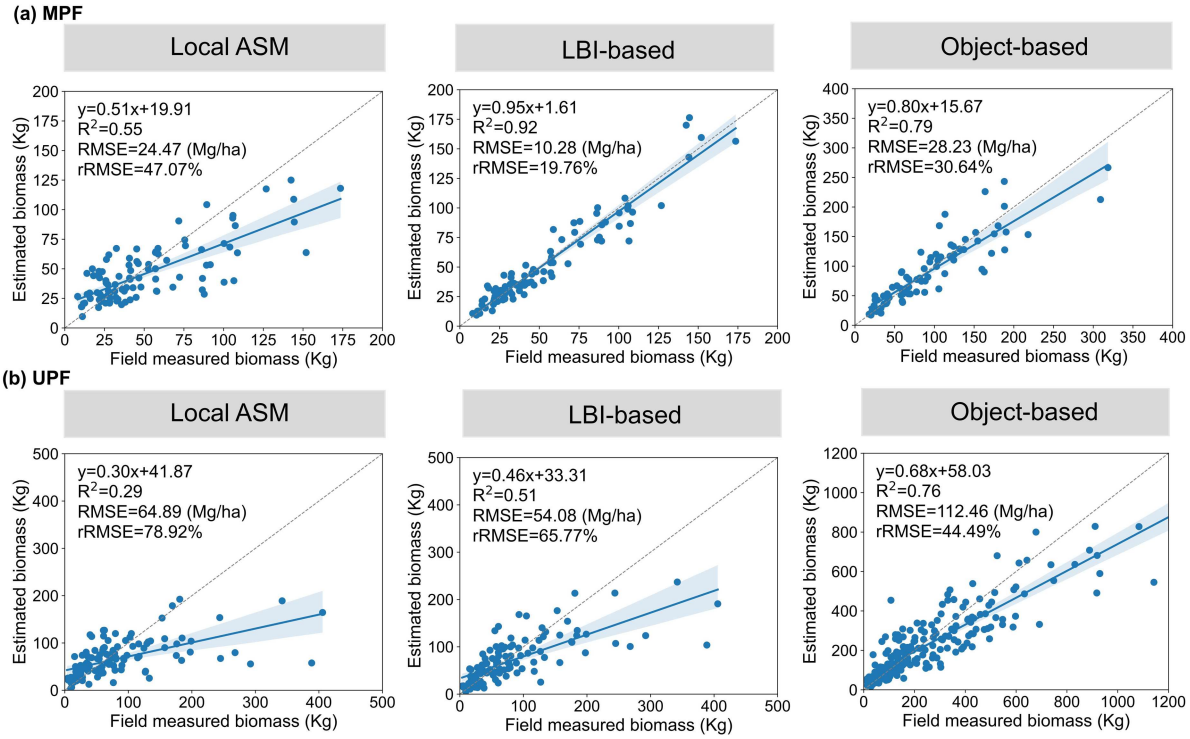

Figure 6. Tree/object level biomass estimation using tree-centric (local ASM and LBI-based) and object-based modelling approaches in the MPF and the UPF.

0.69, respectively (Figure 7a). In the UPF, we found that the object-based approach for plot-level biomass estimation had a lower error than the area-based and tree-centric methods (Figure 7b). The rRMSE values for the object-based, area-based, local ASM, and LBI-based approaches were 21.92%, 26.80%, 41.80%, and 41.25%, respectively. The R^2 values for the object-, area-, local ASM-, and LBI-based approaches were 0.82, 0.73, 0.34, and 0.36, respectively. Overall, all approaches performed better in the MPF, while both the object-based and area-based models provided relatively accurate estimates of plot-level biomass.

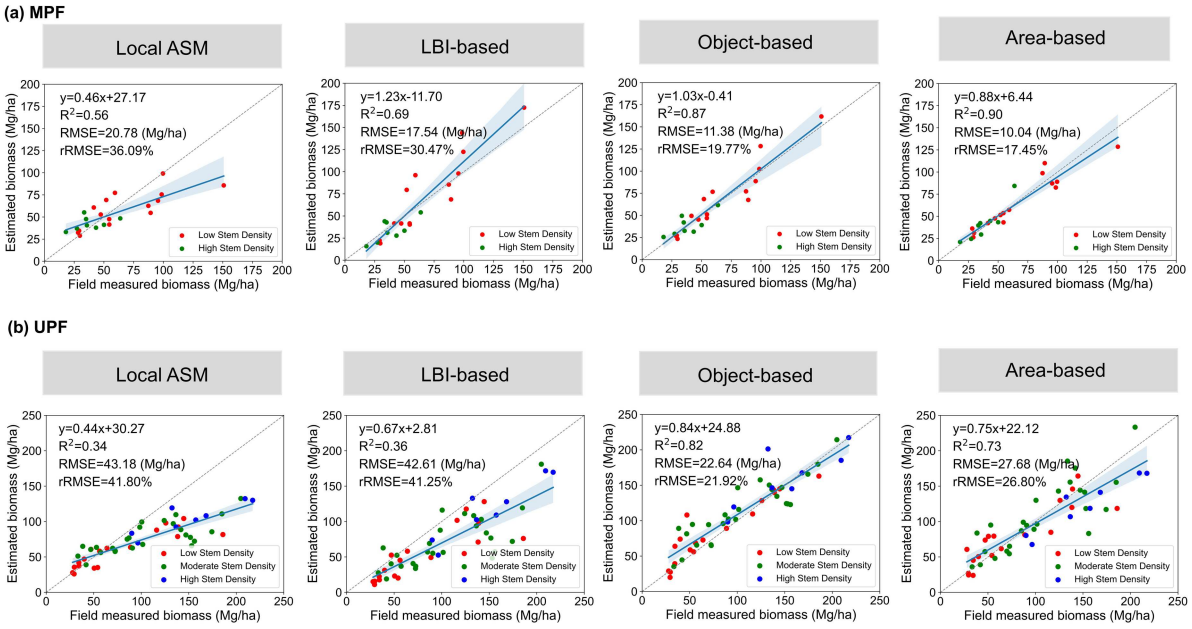

Figure 7. Plot-level biomass estimation using tree-centric (local ASM and LBI-based), object-based and area-based approaches in the MPF and UPF. (MPF: low (<1750 stems/ha), high (≥1750 stems/ha); UPF: low (<1500 stems/ha), moderate (1500–2750 stems/ha), high (≥2750 stems/ha)).

5. Discussion

5.1. *Structural metrics for biomass estimation in forests with different human management types*

In this study, various metrics were calculated for object-based and area-based approaches, and we identified metrics that were important for biomass estimation in forests with different management types.

For the object-based approach, OBI and CE_XY were important in both MPF and UPF. The OBI describes the horizontal and vertical distributions of trees within an object. Capturing understory and overlapping tree information that cannot be fully described by common metrics. Additionally, we introduced canopy entropy, which captures the structural complexity of the forest canopy. The results indicated that canopy entropy in the XY-plane was an effective metric. As noted by Liu et al. (2022), CE estimates in the XY plane are influenced by tree density and tree size, with higher densities and larger trees yielding higher values. Although canopy entropy was designed for forest stands, it is also applicable for objects. Objects with more trees tend to have higher CE_XY values. Consistent with the relationship between biomass, tree number, and tree size (height and DBH). We also observed that in the UPF, voxel-related metrics (μ_{HP75} and μ_{HP10}) were important, while in the MPF, point-based metrics ($Density_{12}$ and $Density_{15}$) were crucial. This is likely related to the impact of human management on the forest structure (Chazdon and Guariguata 2016). In the MPF, intensive management has led to a lack of understory and relative homogeneous canopies (Almeida et al. 2019). Thus canopy height becomes the primary structural attribute, which is captured by point-based metrics $Density_{12}$ and $Density_{15}$. In the UPF, objects generally consist of overlapping or adjacent tree crowns with complex vertical stratification. In the UPF, close-to-nature management allows naturally regenerated forests (Chazdon and Guariguata 2016; Scheeres et al. 2023). Compared to the MPF, the vertical structure of the UPF is more diverse. The object types include not only overlapped trees, but also multistoried trees. Such structural complexity is better captured by voxel-related metrics (μ_{HP75} and μ_{HP10}) Previous studies have demonstrated that voxel-based metrics can improve model generalization for accurate forest attribute predictions (Pearse et al. 2019).

For the area-based approach in the UPF, three metrics remained after the feature selection: μ_{HP75}, σ_{HP75} and LAI. μ_{HP75} and σ_{HP75} are voxel-based metrics that calculate the 75th percentile height within each voxel and summarize it using mean and standard deviation. The advantages of voxel-based metrics were demonstrated by Whelan et al. (2023). They modeled wood volume in longleaf pine woodlands and highlighted that voxel-based metrics outperform area-based metrics in predicting forest attributes in

forests with high structural and compositional variability. Specifically, σ_{CHM} was the most important metric of the area-based model in the MPF. The σ_{CHM} is linked to horizontal heterogeneity in the upper canopy (Camarretta et al. 2020). For even-aged plantation trees with regular spacing, canopy rugosity captures information on stem density, which reflects biomass density.

Generally, metrics that describe vegetation structure and characterize complex forest structures are more important for predicting object biomass, which can be attributed to the structural complexity and diversity of objects. Moreover, human management affects the vegetation structure between the UPF and MPF, resulting in differences in metric selection for biomass modelling. In the MPF, metrics characterizing canopy height and horizontal structure are more important than vertical structure information. In the UPF with complex structures, metrics that consider detailed horizontal and vertical information better account for structural heterogeneity and contribute to more accurate biomass estimations.

5.2. Forest management impacts on biomass estimation

Our results showed that the UAV-LiDAR-driven biomass estimation approaches performed better in the MPF than in the UPF, which is related to differences in forest structure and composition resulting from human management. First, forest structure influences the accuracy of individual tree segmentation in the tree-centric approach. Compared to the MPF with a single species and simple structures, the UPF has high structural and compositional variability (Chazdon and Guariguata 2016; Scheeres et al. 2023). Complex vertical structures affect tree detection in the understory, and crown intersections and irregular crown shapes increase the difficulty of tree detection and crown segmentation. These challenges introduce segmentation errors, which in turn increase uncertainties in tree-centric biomass estimation approaches at both tree and plot levels (Campbell et al. 2023). Second, the biomass modelling of all approaches was affected by differences in human management. Wood density is a key parameter in field-based ASM (Chave et al. 2005), and has been identified as a major source of uncertainty in biomass modelling (Coomes et al. 2017). In the UPF, multiple species with varying wood densities increased the uncertainty of the models. Moreover, the complexity and high variability of the UPF makes it challenging to accurately predict biomass.

Compared to the area-based approach, tree-centric approaches provide fine-scale biomass mapping and are independent of the scale of the calibration plots. Moreover, the model can be developed using only a few trees (Du et al. 2023). However, both in the MPF and UPF, the area-based approaches achieved higher accuracy than the tree-centric approaches, which has been demonstrated in previous studies (Coomes et al. 2017; Campbell et al. 2023). The relatively poor performance of tree-centric approaches can be attributed to individual tree-segmentation errors.

In comparison with tree-centric approaches, the proposed object-based approach performed well in both tree- and plot-level biomass estimation and was less affected by forest management. This suggests that the approach developed in this study is robust and highlights its potential for fine-scale biomass mapping in forests with different types of human management. The robustness of the object-based approach can be explained by two main reasons: (1) the developed object biomass model is composed of OBI and other carefully selected LiDAR-derived metrics, which can fully capture the structural information of objects in both UPF and MPF. (2) The object-based approach mitigates the effects of segmentation errors in the UPF and MPF by treating under-segmented trees as one object.

5.3. Uncertainties and outlook

There are some uncertainties in our study. First, the performance of the OBI may be affected by the point density because some parameters were obtained from the KDE (Liu et al. 2022). The area of crown $A(h)$ in the OBI equation was calculated based on the rasterization of the horizontal point cloud layers. $A(h)$ is the sum of the areas of the grids with density values greater than the 80^{th} percentile in the raster layer. For each grid, a weight was assigned based on the point number in the layer and point density of the grid. Thus, the value of $A(h)$ is affected by point density. Additionally, the value of $W(h)$ might also be influenced by the point density, because the values derived from KDE were directly used in $W(h)$. In our study, LiDAR data were collected during similar flights and a resampling strategy was applied to reduce the impact of point

density. Thus, the influence of point density can be ignored. However, the impact of point density variations on OBI among the study areas needs to be investigated in future studies. Moreover, differences in the topography of the two forests can affect biomass estimation (Khosravipour et al. 2015). We minimized the impact of topography on biomass estimation approaches as much as possible. For instance, we adopted the PTrees algorithm for the UPF to reduce the effect of slope on individual tree segmentation. Compared with topography, large differences in forest structure and composition resulting from forest management are still the main factors affecting biomass estimation. Additionally, due to the lack of sufficient samples with different management approaches and intensities, this study simply divided the planted forest into unmanaged and managed groups. It should be noted that different management approaches (e.g. fertilization, weeding, harvesting) and intensities (minor, medium, and intensive) in planted forests can also alter forest structure and influence biomass estimation (Yu et al. 2020). Further studies are needed for biomass estimation with a more detailed planted forests classification system.

In this study, we investigated the performance of three UAV-LiDAR-driven biomass estimation approaches in the UPF and MPF. The results suggested that the biomass models and their accuracy differed between the UPF and MPF. Compared with tree-centric approaches, the robustness of the developed object-based approach demonstrated its potential for fine-scale biomass mapping in planted forests with different management types. Moreover, our study highlights the impact of human management on biomass estimation. Most previous studies have focused on monoculture plantations and neglected the impact of management types (Yu et al. 2024). Actually, as more attention has been paid to policies to incentivize the improvement of biodiversity in planted forests, there has been a shift in emphasis from monoculture plantations with intensive management to biodiversity-rich mixed forests managed with close-to-nature management (Liu, Wu, and Wang 2014). The neglect of planted forests, such as the UPF, can lead to biased and inaccurate estimations. It is recommended that different management types should be considered for biomass estimation and carbon projection in planted forests, especially for large-scale mapping. Moreover, our results provide a methodological basis for selecting most effective biomass estimation approaches across forest management types, supporting future large-scale mapping and carbon monitoring using UAV-LiDAR or satellite datasets.

6. Conclusion

UAV-LiDAR enables the production of fine detailed point clouds in forests. Our findings demonstrate the differing effectiveness of three UAV-LiDAR-driven biomass estimation approaches across contrasting forest management types. The results showed that: (1) In the UPF with a complex structure, metrics capturing detailed horizontal and vertical information were important for biomass estimation. (2) Both object- and area-based approaches can accurately estimate biomass in the MPF. With increasing structural complexity, the object-based approach outperformed the area-based approach in the UPF. (3) The object-based approach was effective in circumventing the impacts of individual tree segmentation errors, especially in UPF with complex structures.

These findings underscore that forest management significantly shapes structural complexity, which in turn affects the performance of different UAV-LiDAR approaches for biomass estimation. Considering management regimes is therefore essential when retrieving forest attributes at large scales. Moreover, further work is needed to evaluate how different management practices influence estimation accuracy under a more detailed classification of planted forests. By clarifying the strengths and limitations of each approach, our study provides practical guidance for choosing efficient biomass estimation methods, supporting accurate assessments of forest restoration, and informing strategies for the conservation and sustainable management of forest ecosystems.

Geolocation information statement

The study was conducted at planted forests in Fengjie, Chongqing, China (31.249° *N*, 109.142° E) and Zhanjiang, Guangdong, China (20.868° *N*, 109.883° E).

Acknowledgements

This research was funded by the Intergovernmental International Science and Technology Innovation Cooperation Program under the National Key Research and Development Plan (Grant No. 2024YFE0198600), the Director Fund of the International Research Center of Big Data for Sustainable Development Goals (Grant no. CBAS2022DF012), the National Natural Science Foundation of China (Grant No. 42171369 and No. 42522106), and Youth Innovation Promotion Association, Chinese Academy of Sciences (Grant No. Y2022051), the Humboldt Research Fellowship for Experienced Researchers, the National Key Research and Development Project of China (Grant No. 2021YFB3901305), and the Key Deployment Program funded by the Aerospace Information Research Institute Chinese Academy of Sciences (E4Z202021F).

Author contributions

CRedit: Yuwen Fu: Conceptualization, Methodology, Formal analysis, Investigation, Validation, Writing–original draft, writing – review and editing, and visualization; **Wang Li:** Conceptualization, Methodology, Formal analysis, Investigation, Validation, Writing–original draft, writing – review and editing, Visualization, Supervision, Funding acquisition; **Wensheng Duan:** Investigation, Writing – review & editing; **Jie Bai:** Investigation, Writing – review & editing; **Li Wang:** Writing – review & editing, Supervision; **Zheng Niu:** Writing – review & editing, Supervision.

Disclosure statement

No potential conflict of interest was reported by the author(s).

Data availability statement

The data will be made available upon request.

References

Abbasi, A., X. Tang, N. Harris, E. Goldman, J. Gamarra, H. Kim, and W. Luo, et al. 2023. "Spatial Database of Planted Forests in East Asia"*Scientific Data* 10 (1): 1. doi: 10.1038/s41597-023-02383-w.

Akaike, H. 1974. "A New Look at the Statistical Model Identification." *IEEE Transactions on Automatic Control* 19 (6): 6–723. doi: 10.1109/TAC.1974.1100705.

Almeida, D. R. A., S. C. Stark, R. Chazdon, B. W. Nelson, R. G. Cesar, P. Meli, E. B. Gorgens, et al. 2019. "The Effectiveness of Lidar Remote Sensing for Monitoring Forest Cover Attributes and Landscape Restoration." *Forest Ecology and Management* 438 (April): 34–43. doi: 10.1016/j.foreco.2019.02.002.

Bai, J., Y. Zheng Niu, K. Huang, Y. Bi, S. Fu, M. Gao, L. Wu, and Wang. 2024. "Full-Waveform Hyperspectral LiDAR Data Decomposition via Ranking Central Locations of Natural Target Echoes (Rclonte) at Different Wavelengths." *Remote Sensing of Environment* 310: 114227. doi: 10.1016/j.rse.2024.114227.

Bernhard Schmid, Y., M. Loreau, D.I. Forrester, S. Fei, J. Zhu, Z. Tang, and Y. Feng, et al. 2022. "Multispecies Forest Plantations Outyield Monocultures across a Broad Range of Conditions." *Science* 376 (6595): 6595–6868. doi: 10.1126/science.abm6363.

Blackburn, R.C., R. Buscaglia, and A.J. Sánchez Meador. 2021. "Mixtures of Airborne Lidar-Based Approaches Improve Predictions of Forest Structure." *Canadian Journal of Forest Research* 51 (8): 8–1116. doi: 10.1139/cjfr-2020-0506.

Brovelli, M., M. Antonia, F. Crespi, F. Fratarcangeli, E. Giannone, and Realini. 2008. "Accuracy Assessment of High Resolution Satellite Imagery Orientation by Leave-One-out Method." *ISPRS Journal of Photogrammetry and Remote Sensing* 63 (4): 4–440. doi: 10.1016/j.isprsjprs.2008.01.006.

Camarretta, N., P.A. Harrison, T. Bailey, B. Potts, A. Lucieer, N. Davidson, and M. Hunt. 2020. "Monitoring Forest Structure to Guide Adaptive Management of Forest Restoration: A Review of Remote Sensing Approaches." *New Forests* 51 (4): 4–596. doi: 10.1007/s11056-019-09754-5.

Campbell, M.J., J.F. Eastburn, K.A. Mistick, A.M. Smith, and A.E. Stovall. 2023. "Mapping Individual Tree and Plot-Level Biomass Using Airborne and Mobile Lidar in Piñon-Juniper Woodlands." *International Journal of Applied Earth Observation and Geoinformation* 118: 103232. doi: 10.1016/j.jag.2023.103232.

Chave, J., C. Andalo, S. Brown, M. A. Cairns, J. Q. Chambers, D. Eamus, and H. Fölster, et al. 2005. "Tree Allometry and Improved Estimation of Carbon Stocks and Balance in Tropical Forests." *OECOLOGIA* 145 (1): 87–99. doi: 10.1007/s00442-005-0100-x.

Chazdon, R.L., and M.R. Guariguata. 2016. "Natural Regeneration as a Tool for Large-Scale Forest Restoration in the Tropics: Prospects and Challenges." *Biotropica* 48 (6): 6–730. doi: 10.1111/btp.12381.

Coops, N.C., T.R. Piotr Tompalski, M. Goodbody, J.E. Queinnec, D.K. Luther, J.C. Bolton, M.A. White, O.R. Wulder, T. van Lier, and Hermosilla. 2021. "Modelling Lidar-Derived Estimates of Forest Attributes over Space and Time: A Review of Approaches and Future Trends." *Remote Sensing of Environment* 260: 112477. doi: 10.1016/j.rse.2021.112477.

Dalponte, M., and D.A. Coomes. 2016. "Tree-Centric Mapping of Forest Carbon Density from Airborne Laser Scanning and Hyperspectral Data." *Methods in Ecology and Evolution* 7 (10): 10–1245. doi: 10.1111/2041-210X.12575.

Du, L., P. Yong, W. Qiang, H. Chengquan, B. Yu, C. Dongsheng, L. Wei, and K. Dan. 2023. "A LiDAR Biomass Index-Based Approach for Tree- and Plot-Level Biomass Mapping over Forest Farms Using 3D Point Clouds." *Remote Sensing of Environment* 290: 113543. doi: 10.1016/j.rse.2023.113543.

Food and Agriculture Organization. 2020. Global Forest Resources Assessment 2020: Main Report. 2020.

Hulvey, K.B., R.J. Hobbs, R.J. Standish, D.B. Lindenmayer, L. Lach, and M.P. Perring. 2013. "Benefits of Tree Mixes in Carbon Plantings." *Nature Climate Change* 3 (10): 10–874. doi: 10.1038/nclimate1862.

Jeronimo, S.M.A., V.R. Kane, D.J. Churchill, R.J. McGaughey, and J.F. Franklin. 2018. "Applying LiDAR Individual Tree Detection to Management of Structurally Diverse Forest Landscapes." *Journal of Forestry* 116 (4): 336–346. doi: 10.1093/jofore/fvy023.

Jucker, T., T. John Caspersen, J.&A. Chave, C.&A. Antin, N. Barbier, F. Bongers, and M. Dalponte, et al. 2017. "Allometric Equations for Integrating Remote Sensing Imagery into Forest Monitoring Programmes." *Global Change Biology* 23 (1): 1–190. doi: 10.1111/gcb.13388.

Khosravipour, A., A.K. Skidmore, T. Wang, M. Isenburg, and K. Khoshelham. 2015. "Effect of Slope on Treetop Detection using a LiDAR Canopy Height Model." *ISPRS Journal of Photogrammetry and Remote Sensing* 104: 44–52. doi: 10.1016/j.isprsjprs.2015.02.013.

Knapp, N., V. Rico Fischer, A. Cazcarra-Bes, and Huth. 2020. "Structure Metrics to Generalize Biomass Estimation from Lidar across Forest Types from Different Continents." *Remote Sensing of Environment* 237: 111597. doi: 10.1016/j.rse.2019.111597.

Krofcheck, D.J., M.E. Litvak, C.D. Lippitt, and A. Neuenschwander. 2016. "Woody Biomass Estimation in a Southwestern U.S. Juniper Savanna using LiDAR-Derived Clumped Tree Segmentation and Existing Allometries." *Remote Sensing* 8 (6): 453. doi: 10.3390/rs8060453.

Latifi, H., F.E. Fassnacht, J.&A. Müller, A. Tharani, S. Dech, and M. Heurich. 2015. "Forest Inventories by LiDAR Data: A Comparison of Single Tree Segmentation and Metric-Based Methods for Inventories of a Heterogeneous Temperate Forest." *International Journal of Applied Earth Observation and Geoinformation* 42: 162–174. doi: 10.1016/j.jag.2015.06.008.

Li, W., H. Zheng Niu, D. Chen, M. Li, W. Wu, and Zhao. 2016. "Remote Estimation of Canopy Height and Aboveground Biomass of Maize Using High-Resolution Stereo Images from a Low-Cost Unmanned Aerial Vehicle System." *Ecological Indicators* 67: 637–648. doi: 10.1016/j.ecolind.2016.03.036.

Li, W., N. Zheng, S. Rong, Q. Yuchu, W. Li, and C. Hanyue. 2020. "High-Resolution Mapping of Forest Canopy Height Using Machine Learning by Coupling ICESat-2 LiDAR with Sentinel-1, Sentinel-2 and Landsat-8 Data." *International Journal of Applied Earth Observation and Geoinformation* 92: 102163. doi:10.1016/j.jag.2020.102163.

Li, W., W. Guo, M. Pasgaard, Z. Niu, L. Wang, F. Chen, and J. Svenning. 2024. "Unmanaged Naturally Regenerating Forests Approach Intact Forest Canopy Structure but Are Susceptible to Climate and Human Stress." *One Earth* 7 (6): 6. doi: 10.1016/j.oneear.2024.05.002.

Li, W., W. Wang, P. Maya, N. Zheng , W. Li, C. Fang, Q. Yuchu, Q. Hailang, and S. Jens-Christian. 2023. "Human Fingerprint on Structural Density of Forests Globally." *Nature Sustainability* 6 (4): 4. doi: 10.1038/s41893-022-01020-5.

Liang, X., A. Kukko, I. Balenović, N. Saarinen, S. Junttila, V. Kankare, M. Holopainen, et al. 2022. "Close-Range Remote Sensing of Forests: The State of the Art, Challenges, and Opportunities for Systems and Data Acquisitions." *IEEE Geoscience and Remote Sensing Magazine* 10 (3): 32–71. doi: 10.1109/MGRS.2022.3168135.

Liang, X., Y. Wang, J. Pyörälä, M. Lehtomäki, X. Yu, H. Kaartinen, and A. Kukko, et al. 2019. "Forest in situ observations using unmanned aerial vehicle as an alternative of terrestrial measurements." *Forest Ecosystems* 6 (1): 20. doi:10.1186/s40663-019-0173-3.

Liu, S., S. Wu, and H. Wang. 2014. "Managing Planted Forests for Multiple Uses under a Changing Environment in China." *New Zealand Journal of Forestry Science* 44 (1): 1. doi: 10.1186/1179-5395-44-S1-S3.

Liu, X., X. Qin Ma, T. Wu, Z. Hu, L. Liu, Q. Liu, Y. Guo, and Su. 2022. "A Novel Entropy-Based Method to Quantify Forest Canopy Structural Complexity from Multiplatform Lidar Point Clouds." *Remote Sensing of Environment* 282: 113280. doi: 10.1016/j.rse.2022.113280.

Louise Terryn, B., N. Barbier, H.M. Bartholomeus, R. Bartolo, K. Calders, G.&A. Derroire, and B. Brede, et al. 2022. "Non-Destructive Estimation of Individual Tree Biomass: Allometric Models, Terrestrial and UAV Laser Scanning." *Remote Sensing of Environment* 280: 113180. doi: 10.1016/j.rse.2022.113180.

Markus Hollaus, L., E. Lindberg, F. Berger, J. Monnet, M. Dalponte, M. Kobal, and L. Eysn, et al. 2015. "A Benchmark of Lidar-Based Single Tree Detection Methods Using Heterogeneous Forest Data from the Alpine Space." *Forests* 6 (5): 5–1747. doi: 10.3390/f6051721.

Michele Dalponte, D.A., T. Jucker, G.P. Asner, L.F. Banin, D.F. Burslem, S.L. Lewis, and D. A. Coomes, et al. 2017. "Area-Based vs Tree-Centric Approaches to Mapping Forest Carbon in Southeast Asian Forests from Airborne Laser Scanning Data." *Remote Sensing of Environment* 194: 77–88. doi: 10.1016/j.rse.2017.03.017.

Næsset, E., and K. Bjerknes. 2001. "Estimating Tree Heights and Number of Stems in Young Forest Stands Using Airborne Laser Scanner Data." *Remote Sensing of Environment* 78(3): 3–340. 10.1016/S0034-4257(01)00228-0.

Pearse, G.D., M.S. Watt, J.P. Dash, C. Stone, and G. Caccamo. 2019. "Comparison of Models Describing Forest Inventory Attributes Using Standard and Voxel-Based Lidar Predictors across a Range of Pulse Densities." *International Journal of Applied Earth Observation and Geoinformation* 78: 341–351. doi: 10.1016/j.jag.2018.10.008.

Qi, Y., N.C. Coops, L.D. Daniels, and C.R. Butson. 2022. "Comparing Tree Attributes Derived from Quantitative Structure Models Based on Drone and Mobile Laser Scanning Point Clouds across Varying Canopy Cover Conditions." *ISPRS Journal of Photogrammetry and Remote Sensing* 192: 49–65. doi: 10.1016/j.isprsjprs.2022.07.021.

Roussel, J., N.C. David Auty, P. Coops, T.R. Tompalski, A.S. Goodbody, J. Meador, F. Bourdon, A. de Boissieu, and Achim. 2020. "lidR: An R Package for Analysis of Airborne Laser Scanning (ALS) Data." *Remote Sensing of Environment* 251 (December): 112061. doi: 10.1016/j.rse.2020.112061.

Scheeres, J., J. Johan de Jong, B. Brede, P.H. Brancalion, E.N. Broadbent, A.M.A. Zambrano, and E.B. Gorgens, et al. 2023. "Distinguishing Forest Types in Restored Tropical Landscapes with UAV-Borne LIDAR." *Remote Sensing of Environment* 290 (May): 113533. doi: 10.1016/j.rse.2023.113533.

Shi, Y., A.K. Tiejun Wang, M. Skidmore, and Heurich. 2018. "Important LiDAR Metrics for Discriminating Forest Tree Species in Central Europe." *ISPRS Journal of Photogrammetry and Remote Sensing* 137: 163–174. doi:10.1016/j.isprsjprs.2018.02.002.

Shirong Liu, Z., H. Li, J. Liang, W. Liu, S. Piao, H. Tian, and Z. Yu, et al. 2024. "Maximizing Carbon Sequestration Potential in Chinese Forests through Optimal Management." *Nature Communications* 15 (1): 1. doi: 10.1038/s41467-024-47143-5.

Thomas Kastner, K., C. Plutzar, A.L.S. Bais, N. Carvalhais, T. Fetzel, S. Gingrich, and K. Erb, et al. 2018. "Unexpectedly Large Impact of Forest Management and Grazing on Global Vegetation Biomass." *Nature* 553 (7686): 7686. doi: 10.1038/nature25138.

Vandendaele, B., R.A. Fournier, U. Vepakomma, G. Pelletier, P. Lejeune, and O. Martin-Ducup. 2021. "Estimation of Northern Hardwood Forest Inventory Attributes Using UAV Laser Scanning (ULS): Transferability of Laser Scanning Methods and Comparison of Automated Approaches at the Tree- and Stand-Level." *Remote Sensing* 13 (14): 14. doi: 10.3390/rs13142796.

Vega, C., A. Hamrouni, S. El Mokhtari, J. Morel, J. Bock, J.-P. Renaud, M. Bouvier, and S. Durrieu. 2014. "PTrees: A Point-Based Approach to Forest Tree Extraction from Lidar Data." *International Journal of Applied Earth Observation and Geoinformation* 33: 98–108. doi: 10.1016/j.jag.2014.05.001.

Wang, Q., D. Yong Pang, X. Chen, J. Liang, and Lu. 2021. "Lidar Biomass Index: A Novel Solution for Tree-Level Biomass Estimation Using 3D Crown Information." *Forest Ecology and Management* 499: 119542. doi: 10.1016/j.foreco.2021.119542.

Whelan, A.W., J.B. Cannon, S.W. Bigelow, B.T. Rutledge, and A.J. Sánchez Meador. 2023. "Improving Generalized Models of Forest Structure in Complex Forest Types Using Area- and Voxel-Based Approaches from Lidar." *Remote Sensing of Environment* 284: 113362. doi: 10.1016/j.rse.2022.113362.

Yu, Z., Z. Hongrun Zhao, S. Liu, G. Zhou, J. Fang, G. Yu, X. Tang, and H. Zhao, et al. 2020. "*Mapping Forest Type and Age in China's Plantations*." Science of The Total Environment 744: 140790. doi: 10.1016/j.scitotenv.2020.140790.

Zhang, J., M. Bojie Fu, S. Stafford-Smith, W. Wang, and Zhao. 2021. "Improve Forest Restoration Initiatives to Meet Sustainable Development Goal 15." *Nature Ecology Evolution* 5 (1): 1–13. doi: 10.1038/s41559-020-01332-9.

Zhang, W., P. Jianbo Qi, H. Wan, D. Wang, X. Xie, G. Wang, and Yan. 2016. "An Easy-to-Use Airborne LiDAR Data Filtering Method Based on Cloth Simulation." *Remote Sensing* 8 (6): 501. doi: 10.3390/rs8060501.